ISSN (Print) 1598-5385
ISSN (Online) 2233-6648
≪연구논문≫ Journal of the Korean Magnetics Society 36(2), 144-148 (2026) https://doi.org/10.4283/JKMS.2026.36.2.144

Structural and Magnetic Study of Liquid-Nitrogen-Quenched $MnFe_2O_4$

Sunghyun Yoon*
Department of Physics, Gunsan National University, Gunsan 54150, Korea

(Received 3 February 2026, Received in final form 11 March 2026, Accepted 12 March 2026)

We have studied structural and magnetic properties of standard bulk $MnFe_2O_4$ by using XRD, SQUID, XPS, and ^{57}Fe Mössbauer spectroscopy throughout wide temperature range from 20 K up to magnetic transition temperature. High-quality bulk sample was prepared by employing a conventional ceramic method followed by rapid liquid nitrogen quenching through which we could avoid the creation of unnecessary secondary phase. Furthermore, we tried to keep the consistency in measurements by obtaining the Mössbauer spectra using single spectrometer all along the temperatures examined. By taking account of both the facts that the B-site Fe^{3+} ion could have various cations (Mn and Fe) neighbor distribution and that the inversion degree of the sample was low, we could satisfactorily analyze the data and explain the temperature behavior of Mössbauer parameters.

Keywords : ^{57}Fe Mössbauer spectroscopy, manganese ferrite, neighboring cation distribution, liquid nitrogen quenching

액체질소 급랭법으로 만든 $MnFe_2O_4$의 구조적 및 자기적 특성 연구

윤성현*
국립군산대학교 반도체물리학과, 군산시 대학로 558, 54150

(2026년 2월 3일 받음, 2026년 3월 11일 최종수정본 받음, 2026년 3월 12일 게재확정)

표준 $MnFe_2O_4$ 시료의 구조적 및 자기적 특성을 XRD, SQUID, XPS 및 ^{57}Fe Mössbauer 분광법을 사용하여 20 K에서 자기 전이 온도까지의 넓은 온도 범위에 걸쳐 연구했다. 고품질 덩어리 샘플은 기존의 세라믹 방법을 사용하여 합성한 후 액체 질소를 빠르게 급랭하여 불필요한 2차 상의 생성을 피했다. 또한, 조사된 모든 온도에 걸쳐 단일 분광기를 사용하여 Mössbauer 스펙트럼을 얻음으로써 측정의 일관성을 유지하고자 했다. B-자리 Fe^{3+} 이온이 다양한 인접 양이온(Mn 및 Fe) 분포를 가질 수 있고 샘플의 반전 정도가 낮다는 사실을 이용함으로써 만족스러운 데이터 분석과 Mössbauer 매개변수의 온도 거동 설명이 가능했다.

주제어 : ^{57}Fe 뫼스바우어 분광학, 망간 페라이트, 인접 양이온분포, 액체질소 급랭

I. Introduction

Oxide spinel is one of vast oxide groups containing transition metal ions, where the tetrahedral (A) sites and the octahedral (B) sites are among the face-centered close packed array of 32 oxygen ions. Of these, only 8 tetrahedral sites and 16 octahedral sites are occupied by metal atoms, making up 8 molecules in the formula of AB_2O_4, that is, 56 atoms form unit cells. Manganese ferrites have been extensively investigated as potential materials for supercapacitors and batteries [1], electrodes [2], catalysts [3], carbon reduction [4], pollutant remediation [5]. Their properties are known to vary dramatically due to the critical impacts of the morphology, crystal, magnetic structures, and the site occupancy and valence states of the constituent transition metals. Previous studies have shown that $MnFe_2O_4$ is a ferrimagnetic cubic mixed spinel. Tetrahedral and octahedral site preference of Mn^{2+} and Mn^{3+} ions bring about the formula $(Mn^{2+}_{1-y}Fe^{3+}_{y})[Mn^{3+}_{y}Fe^{2+}_{y}Fe^{3+}_{2-2y}]O_4$ (y = degree of

*Corresponding author: Tel: +82-63-469-4562, +82-10-4781-1087, E-mail: shyoon@ksnu.ac.kr

inversion), where the parenthesis and square bracket represent the tetrahedral (A-) and the octahedral (B-) sites, respectively [6,7].

Most of recent studies have focused mainly on materials of high functional forms, i.e., nanoparticles or thin films, so the effects such as superparamagnetism and inter-grain interactions overwhelm the fundamental properties of materials [8-10]. In this study, high-quality bulk sample has been synthesized and the its Mössbauer spectroscopic characteristics are investigated. In particular, by carrying out measurements from low temperatures to magnetic transition temperature T_N with a single spectrometer, we intend to ensure the consistency of the measurements and to find out the consistent characteristic variations over a wide range of temperatures.

II. Experiments

The $MnFe_2O_4$ sample used in this study were synthesized by a conventional solid-state reaction followed by liquid nitrogen (LN2) quenching. Appropriate amounts of MnO, and Fe_2O_3 powders was mixed with agate and pestle, compressed into a pellet, heat-treated at 1,100 ºC in air, and subsequently dropped into boiling LN2. This method has a benefit of avoiding the generation of secondary phase during the cooling stage [11]. In order to confirm the crystal structure of the synthesized sample, a powder X-ray diffraction (XRD) pattern using Cu$K\alpha$ radiation was obtained at room temperature. In order to investigate the macroscopic magnetic properties, the magnetic hysteresis curve was obtained in the ±1 T range using a vibrating sample magnetometer (VSM) at room temperature, and the saturated magnetization M_S, the coercive force H_C, and the magnetic anisotropy constant K were obtained. Charge states of constituent ions were monitored by X-ray photoemission spectroscopy (XPS). In order to examine the microscopic magnetic properties at the atomic scale, Mössbauer spectra have been taken from 20 K up to magnetic transition temperature using a conventional transmission-type spectrometer using ^{57}Co source diffused in the rhodium matrix at room temperature. All velocity scales were calibrated using α-Fe foil.

III. Results and Discussion

Rietveld refinement using the GSAS package was performed on the powder XRD profile of the synthesized sample, and the result of analysis is shown in Fig. 1. The diffraction pattern was consistent with previously published studies [12], and the sample showed no traces of impurities. It was confirmed that the sample had a cubic structure with a space group Fd/3m and its lattice constant was a = 8.51245 Å. Fig. 2 depicts interatomic bond lengths and angles for A- and B-sites of the sample. While the A-site was regular tetrahedron, octahedral site showed trigonal distortion along [111] direction despite its structure is overall cubic.

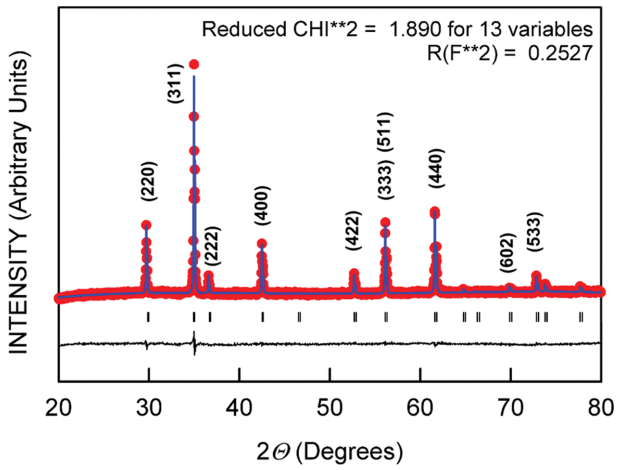

Fig. 1. (Color online) GSAS refinement of $MnFe_2O_4$ prepared by LN2 quenching.

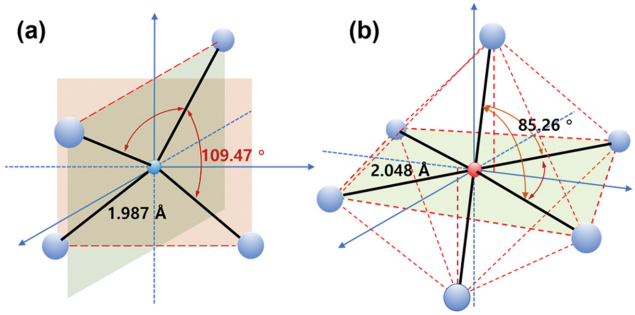

Fig. 2. (Color online) Local coordination of A- and B-site in $MnFe_2O_4$ prepared by LN2 quenching.

Fig. 3 shows the room-temperature M-H curve of $MnFe_2O_4$. By fitting the high-field part of the hysteresis curve to the law of approach to saturation, we could get the optimum values of saturation magnetization M_S = 81.2 emu/g and magnetic anisotropy constant $K = 1.09 \times 10^5$ J/m^3 which fall in the ranges reported by previous studies [13]. Coercive force H_C was as low as 40 G indicating that the sample is already in multi-domain criteria due to its high sintering temperature. Fig. 4 displays the XPS analysis results of $MnFe_2O_4$ samples. It is noticeable that considerable amounts of Fe^{2+} and Mn^{3+} present despite the normal spinel nature of $MnFe_2O_4$ by which Mn^{2+} and Fe^{3+} have been reported to preferentially occupy the A- and B-site, respectively [14].

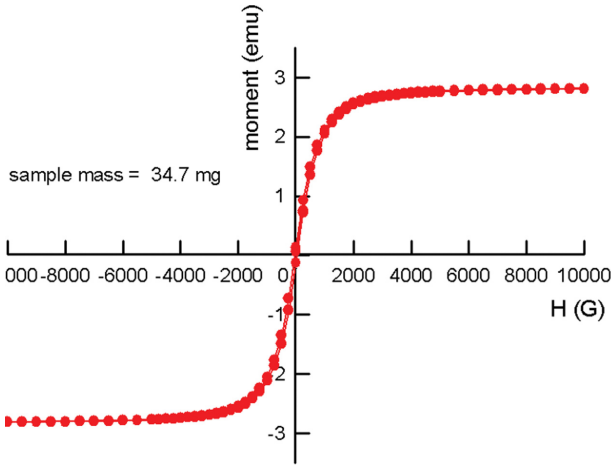

Fig. 3. (Color online) Room-temperature *M-H* curve of $MnFe_2O_4$ prepared by LN2 quenching.

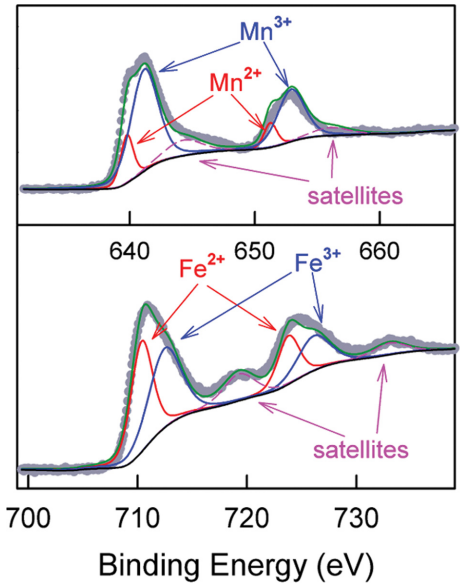

Fig. 4. (Color online) Results of XPS analysis for $MnFe_2O_4$ prepared by LN2 quenching.

Mössbauer spectra taken from 20 K to the paramagnetic transition temperature could be fitted by the superpositions of two sub-spectra stemming from the A- and the B-sites, which means this sample is not a perfect normal spinel. In the composition of $MnFe_2O_4$ where there are twice as many B-sites as A-sites, it is not possible that the absorption area of A-site exceeds that of B-site. Therefore, we can ascribe the smaller sub-spectrum with larger hyperfine magnetic field to Fe^{3+} ions at A-site, whereas the other major sub-spectrum to those at B-site. Given the inversion degree x, the probability for an Fe^{3+} ion at B-site to have n A-site Fe^{3+} ions as nearest neighbors $P(x, n)$ (n = 0 to 6) is given by the following

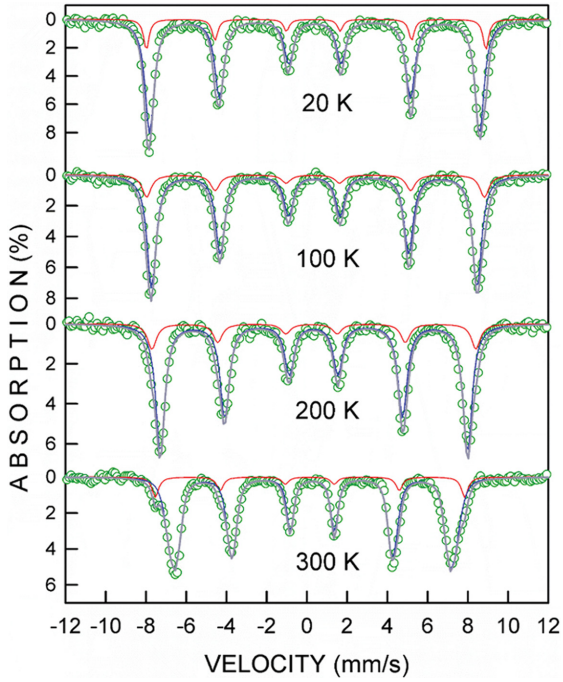

Fig. 5. (Color online) Typical Mössbauer spectra of the $MnFe_2O_4$ sample taken at low temperatures.

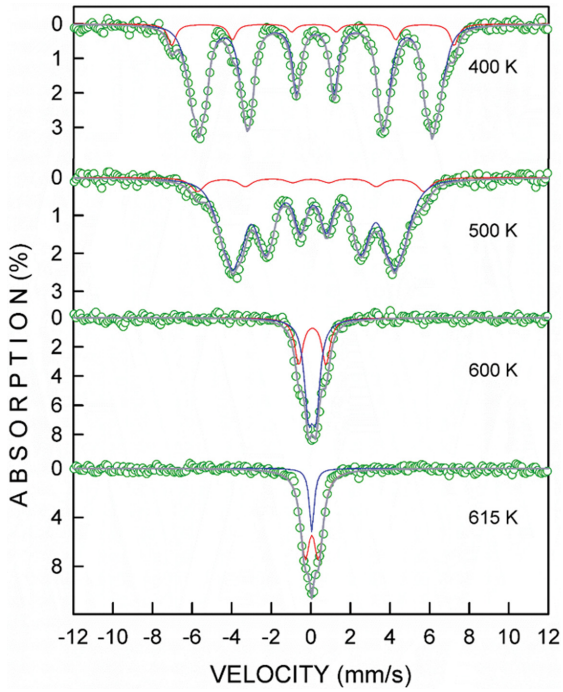

Fig. 6. (Color online) Typical Mössbauer spectra of the $MnFe_2O_4$ sample taken at high temperatures.

binomial distribution function:

$$P(x, n) = {}_6C_n\, x^n\, (1 - x)^{6-n} \quad (1)$$

Then the magnetic hyperfine field at B-site Fe^{3+} nucleus with

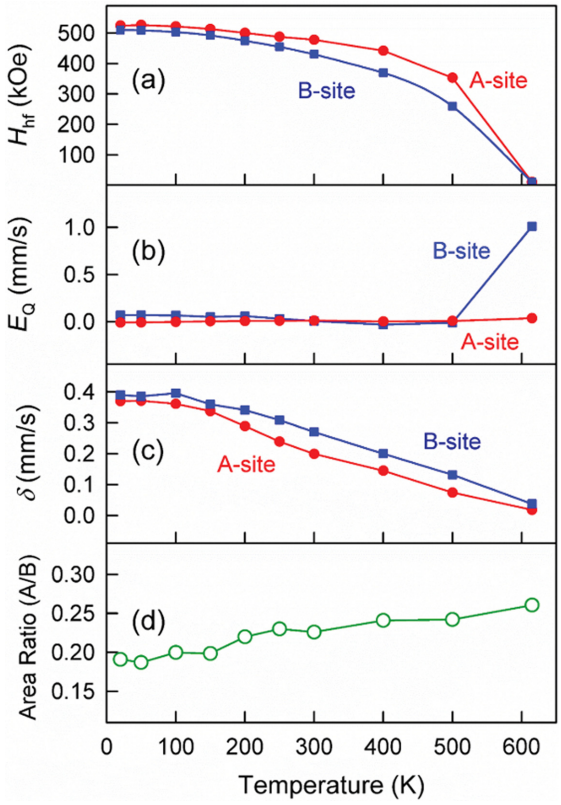

Fig. 7. (Color online) Temperature variation of Mössbauer parameters of $MnFe_2O_4$ prepared by LN2 quenching.

n Fe^{3+} neighbors can be written simply as $H_0 - (6-n)\Delta H$ where H_0 and ΔH were fitting parameters. Since the inversion degree x is low, the A-site sextet was presumed to be a single component. Superposing these component spectra from multiple environmental configurations of Fe^{3+} ions with the weight of $P(x, n)$, we can get resultant spectra as illustrated in Figs. 5 and 6. Néel temperature T_N was taken as a temperature where the sextets collapsed and singlet (or doublet) emerged. From Fig. 5, a spectrum taken at 600 K looks an overlap of doublet with a narrow sextet. With further increasing the temperature, however, a spectrum composed of a singlet and a doublet observed at 615 K. As has been mentioned in Fig. 2, the singlet and the doublet originate from Fe^{3+} ion located at the regular tetrahedron and the trigonally distorted octahedron, respectively.

Fig. 7 depicts temperature variation of various Mössbauer parameters. Throughout the whole temperature range examined, the magnetic hyperfine field H_{hf} of A-site was found out to be stronger than that weigh-averaged for B-site. Some previous studies of $MnFe_2O_4$ have reported that the hyperfine field of B-site is generally stronger than that of A-site [15]. In this spinel structure, however, the A-site comprised 12 B-site neighbors while the B-site comprised 6 A-site neighbors. When the inversion degree x is low, B-site Fe^{3+} ions do not have sufficient number of A-site Fe^{3+} ions as neighbors, which could lead to the relation $H_{hf}(A) > H_{hf}(B)$. For all the temperatures, the electric quadrupole splitting E_Q values of A-site was effectively zero because its local symmetry was regular tetrahedral coordination. As can also be seen from Fig. 7(b), however, the low temperature subspectra of B-site were fitted well with zero E_Q despite the trigonally distorted structure while we can observe doublet of non-zero E_Q above T_N. This discordance can be explained as follows: when there exists magnetic order, E_Q could be averaged to zero as the principal axes of EFG tensor could take any direction with respect to hyperfine magnetic field. Non-zero E_Q has been observed as soon as the hyperfine magnetic field disappeared. Isomer shift values in Fig. 7(c) indicated that the valences of iron ions were all trivalent. In contrast to the XPS results. the isomer shift values revealed that no traces of Fe^{2+} were identified. This could possibly be due to the different measuring time windows of Mössbauer spectroscopy (~10^{-10} s) and X-ray spectroscopy (~10^{-15} s). [16] Finally, as can be calculated from Fig. 7(d), the inversion degree retains ~0.37 all the way through the temperature examined.

IV. Conclusion

We have synthesized high quality $MnFe_2O_4$ powder sample through a solid-state reaction followed by a rapid LN2 quenching. XRD showed that the $MnFe_2O_4$ had a cubic spinel structure though the local symmetry of the B-site was trigonally distorted along [111] direction. Result of VSM measurement showed ferrimagnetic behavior with M_S = 81.2 emu/g, K = 1.09 × 10^5 J/m^3, and H_C = 40 G, respectively. XPS analysis showed the presence of Fe^{2+} and Mn^{3+} ionic state. Mössbauer spectra were analyzed as a sum of contributions from possible neighboring Fe^{3+} ion distribution around each site. Due to the neighboring Fe^{3+} distribution and low inversion degree, hyperfine magnetic field at A-site was stronger than that of B-site. Isomer shift values indicated that the ionic valence of iron was only +3, which is in contrast to the result of XPS. Ratio of absorption area indicated that the inversion degree maintained ~0.37.

References

[1] D. Abisha, S. R. Gibin, V. K. PremKumar, and A. Mariappan, Heliyon **9**, e21120 (2023).

[2] R. P. Bhosale, S. S. Kumbhar, S. B. Bhosale, R. R. Salunkhe, V. A. Kadam, S. P. Pardhi, S. S. Gholap, C. D. Lokhande, and V. S. Jamadade, J. Energy Storage **86** Part A, 111146 (2024).
[3] C. Qi, Q. Liu, Y. Dong, G. Zhang, X. Jiang, and D. Gao, RSC Adv. **12**, 27206 (2022).
[4] J. Wang, Z. Su, T. Zhang, and T. Jiang, Chem. Eng. J. **479**, 147926 (2024).
[5] M. E. C. Ferreira, E. G. Bernardino, M. A. S. D. de Barros, R. Bergamasco, and N. U. Yamaguchi, J. Water Process. Eng. **54**, 104049 (2023).
[6] M. Tanaka and T. Mizoguchi, J. Phys. Soc. Jpn. **18**, 1091 (1963).
[7] V. A. M. Brabers, J. Phys. Chem. Solids **32**, 2181 (1971).
[8] N. S. Gajbhiye, G. Balaji, and M. Ghafari, Phys. Sol. Solidi (a). **189**, 357 (2002).
[9] C. Simon, A. Blösser, M. Eckardt, H. Kurz, B. Weber, M. Zobel, and R. Marschal, Z. Anorg. Allg. Chem. **647**, 2061 (2021).
[10] P. Rajagiri, B. N. Sahu, N. Venkataramani, S. Prasad, and R. Krishnan, AIP Adv. **8**, 056112 (2018).
[11] S. Yoon, AIP Adv. **15**,035308 (2025).
[12] C. Y. Gao, E. Baek, C. Y. You, and H. J. Choi, Colloid and Polymer Science **299**, 865 (2021).
[13] B. Aslibeiki, P. Kameli, and M. H. Ehsani, Ceramics International **42**, 12789 (2016).
[14] Y. Xiao, D. E. Wittmer, F. Izumi, S. Mini, T. Graber, and P. J. Viccaro, Appl. Phys. Lett. **85**, 736 (2004).
[15] S. Wen, B. Chen, J. Zhang, W. Zhan, Z. He, and L. Gao, Crystals **13**, 1509 (2023).
[16] W. Fu, H. Cai, D. Wang, Y. Lei, and J. Liu, Optik - International Journal for Light and Electron Optics **186**, 374 (2019).